MIXED BOUNDARY VALUE PROBLEM IN MICROFLUIDICS: THE AVER'YANOV–BLUNT MODEL REVISITED

ANVAR KACIMOV [1] and YURII OBNOSOV [2]

Abstract

Macroscopically, a Darcian unsaturated moisture flow in the top soil is usually represented by an one-dimensional volume scale of evaporation from a static water table. On the microscale, simple pore-level models posit bundles of small-radius capillary tubes of a constant circular cross-section, fully occupied by mobile water moving in the Hagen–Poiseuille (HP) regime, while large-diameter pores are occupied by stagnant air. In our paper, cross-sections of cylindrical pores are polygonal. Steady, laminar, fully developed two-dimensional flows of Newtonian water in prismatic conduits, driven by a constant pressure gradient along a pore gradient, are more complex than the HP formula; this is based on the fact that the pores are only partially occupied by water and immobile air. The Poisson equation in a circular tetragon, with no-slip or mixed (no-shear-stress) boundary conditions on the two adjacent pore walls and two menisci, is solved by the methods of complex analysis. The velocity distribution is obtained via the Keldysh–Sedov type of singular integrals, and the flow rate is evaluated for several sets of meniscus radii by integrating the velocity over the corresponding tetragons.

1. Introduction

The motivation to apply microfluidic models to the hydrology of "solonchaks" is presented in this section. The fluxes of all pore fluids (liquid H_2O and soil gases) in the topsoil, especially in the vadose zone, are of utmost importance in soil hydrology,

---

[1] Sultan Qaboos University, Seeb, Sultanate of Oman; e-mail: anvar@squ.edu.om, akacimov@gmail.com
[2] Kazan Federal University and Institute of Forest Science, Russian Academy of Sciences, Moscow, Russia; e-mail: yobnosov@kpfu.ru

civil engineering and agro-environmental management of soil resources, in particular
in hot dry lands [23]. In arid deserts, the topsoil is usually very dry and the water
table is deep (5+ m), that is, evaporation is negligible. However, at many urban
locales of the Middle Eastern and North African countries, a new phenomenon of
shallow (perched) water tables was recently discovered and mathematically modelled
[7, 20]. The capillary fringe of these aquifers is a zone extensively emitting water
by evapotranspiration to the desert atmosphere. This zone is only 10 to 50 cm
thick. Mitigating the catastrophic consequences of waterlogging is imperative for the
governments and public in the affected regions, especially in the urbanized catchment
of Oman and the other Gulf countries. Dialectically, there are also ecohydrologically
benign effects of shallow water tables (in particular, if groundwater is brackish or
saline): for example, phreatophytes and halophytes thrive and deposit/sequester CO_2
(see [19]). The main question that soil physicists have to answer is: "How does one
evaluate the ascending flux of moisture from a shallow, almost static, water table"?

We recall that direct measurements of evaporation require buried lysimeters (not
used in Oman and other Gulf countries), which are expensive and cumbersome. In
Australia, where shallow water tables and the ensuing waterlogging became a national
disaster in the 1970s [33], the measured moisture fluxes (maintained by evapotranspira-
tion and conceptualized as one-dimensional on the representative elementary volume
(REV) scale) were 500+ mm/year, that is, hydrologically huge. Similarly, in the USSR
(Central Asia) irrigation engineers confronted similar hyperintensive evaporation and
salinization of agricultural lands [5]. The microfluidic models of this process were,
however, not developed by Australians or Soviets.

Our paper analyses the microscopic process of two-dimensional pore water motion,
which takes place in desert soils classified as "solonchaks" ("sabkhas" in Arabic)
[11, 23]. The analytic solutions give integral representations (Keldysh–Sedov type
[18]) via singular integrals for an analytic function, found in a canonical domain
(half-plane). Modelling of the pore water dynamics at this scale can be an overture to
further field measurements of moisture motion in thin vadose zones and to developing
the means of optimally controlling the macroscopic evapotranspiration.

The monitoring of perched aquifers in Oman [2] evidenced that the depth of
the water table in most of them is not only small but also almost constant. Conse-
quently, although the atmospheric conditions vary with seasons, the annually averaged
evaporation flux in our model is assumed to be steady state. We also assume that
the mobile soil water phase is continuous, that is, it moves within soil pores under
a constant pressure gradient, whereas the air phase is static. In soil physics, most
models assume connected moisture pathway flow at the pore scale that implies
the functional form of the two-phase Darcy equations. In problems with rapidly
fluctuating water tables caused by, for example, infiltration, rather than evaporation, the
water retention functions and water relative permeability are dynamic (in particular,
hysteretic), that is, associated with rapidly moving breathing menisci and water–air
contact lines. The rapidity of infiltration of irrigated water into the topsoil, as well

as the propagation of the oil–water contacts in secondary recovery of crude oils in formations [9], are very different from the "rapidity" of salinization, as pinpointed by Aver′yanov [5]. A typical timescale of infiltration is minutes and hours, while for Aver′yanov″s evaporative fluxes and the ensuing primary/secondary salinization and hydromorphism of "solonchaks" it is months and years.

Macroscopically, such flows are classified as "variably saturated" (see [3, Section 6.2] for more details), and obey the Richards–Richardson [28] nonlinear parabolic partial differential equation (PDE), which can be solved analytically for steady-state flows, as in two-dimensional evaporation in the vicinity of either a ponded land surface (application to flood irrigation [35]) or an impeding surface (buildings foundation in urban hydrology [10]). In case of transient seepage, the PDE is numerically solved. On the pore scale, water motion obeys the Navier–Stokes PDE, which, under the simplifications of our model, is reduced to the Poisson equation [6, 31].

Models for relative permeabilities of the water k_{rw} and air k_{ra} phases in macroscopically (REV-scale) two-phase steady-state Darcian flows through porous media are applied in soil physics, and in reservoir, geotechnical and chemical engineering. In these models, semi-empirical dependencies of k_{rw} and k_{ra} on the degrees of saturation with respect to water, S_w, or on the capillary pressure (matric potential/suction) head, p, are used [9, 13, 16, 24]). In the Richards–Richardson PDE for the mobile phase only, the functions $k_{rw}(S_w)$ or $k_{rw}(p)$ were developed in [5, 16, 25] among others. On a microscale, Aver′yanov [4] considered a partially filled circular pore and solved the Poisson equation (see, for example, [26] for details of Aver′yanov″s derivations) in an annulus with a no-slip condition for water velocity along the pore wall (a circle with a large radius) and a no-shear condition along a meniscus (a concentric circle with a smaller radius). Aver′yanov found that $k_{rw} = k_w/k_0 = S_w^{m_A}$, where $0 \leq S_W \leq 1$, and k_w and k_0 are the unsaturated and saturated (intrinsic) hydraulic conductivities of the soil, respectively. Aver′yanov″s analytically derived exponent $m_A \approx 3.5$ (see further empirical analysis in [12, 29]) is consistent with the empirical Campbell analysis, which was obtained for pores of various radii but fully occupied by capillary water. The Van Genuchten relative permeability function [28] for pore water is

$$k_{rw} = S_w^{1/2}\{1 - (1 - S_w^{1/m_{VG}})^{m_{VG}}\}^2,$$

where m_{VG} is a soil-specific empirical constant. Aver′yanov″s exact and explicit solutions were generalized to the case of two Poisson equations in [14], where the conjugation condition was imposed on a circular interface (meniscus), which separates water and oil phases concurrently moving in a steady-state regime.

In our view, there is an issue with the REV versus pore-level upscaling–downscaling: bundles of conduits are most often postulated to be circles (in their cross-sections perpendicular to the macroscopic pressure gradient). The real pore channels are obviously not circular, even if cylindrical. Such "circularization" of water conduits stems, obviously, from the availability of the Hagen–Poiseuille (HP) formula [3] for a one-phase flow through a pipe. In unsaturated moisture flow models [28], microscopic
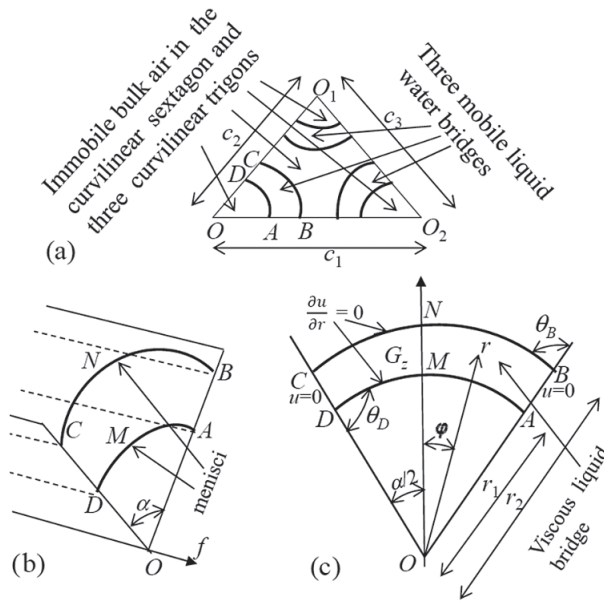
FIGURE 1. (a) Cross-section of an arbitrary triangular pore. Three thin mobile water "bridges" are sandwiched between immobile air. (b) 3D diagram with zoomed menisci CNB and DMA near one pore corner. (c) Boundary conditions in the flow domain, a circular tetragon G_z.

tubes of sufficiently small radii are believed to convey the pore water in the HP regime, while the air is static in large-diameter empty pores. In transient quasi-HP regimes of rapid imbibition/drainage, for example, in the Green–Ampt infiltration model [24], the HP formula is usually adjusted by assuming a propagating meniscus.

Microfluidic models (see Figures 2.16, 3.4, 3.6, 4.1, 4.2 and 5.5 in [9]) consider polygons (triangles and rectangles) rather than circles as cross-sections of the pore channels making parallel bundles. The vertices of these polygons (angular pores) allow accumulation of the water phase in the crevices of pores (the case tackled by Kacimov et al. [22]) or in water "bridges", sandwiched between immobile bulk air phases by two zero-shear stress menisci (see Figures 2.29, 5.6 and 5.16 in [9] and our Figure 1).

In this paper, we use the theory of holomorphic functions [17, 18], and we obtain a new integral solution to a mixed boundary value problem (BVP) for the Poisson equation in a circular quadrangle G_z, as shown in Figure 1, which has zero pore velocity on the straight sides of the quadrangle and zero-shear boundary condition on two menisci. In other words, our paper is a confluence of the Aver′yanov combination of the boundary conditions (tackled analytically) with Blunt′s more realistic geometry of pore cross-sections.

We recall that an area integration of the Prandtl function, which also obeys the Poisson equation, gives a torsional rigidity of an elastic bar [34]. In microfluidics, a mathematically equivalent integration of the magnitude of the pore water velocity over G_z gives the volumetric discharge, provided the air phase is stagnant. In Section 2, a

mixed (no-slip versus no-shear conditions) BVP is solved in a curvilinear quadrangle for the Poisson equation, which the velocity of the water phase obeys. The moisture content within the triangular pores is relatively low and the air phase is static. In Section 3, the obtained solution is interpreted as an approximation of water flow in the case of high moisture content and stagnant air confined near the corners of the pore, as well as for the case of the dominating gas phase flowing through the bulk volume of the pores, while the immobile water phase is trapped near the corners. In Section 4, the limitations and perspectives of our analytical model are discussed.

2. Analytical solution to a mixed BVP, Poisson''s PDE

In a cross-section perpendicular to the macroscopically vertical direction Of (ascending evaporation), we assume that the pore makes a triangle OO_1O_2 having arbitrary sides c_1, c_2, c_3, (Figure 1(a)). As a geometrical input of our model, we consider the vicinity of one corner (O) of this triangle where water is contained in a "bridge" bounded by two menisci, AMD and CNB, and two pore walls making an angle α, $0 < \alpha < \pi$ (Figure 1(b)). The menisci are circular arcs of constant radii, r_1 and r_2, respectively. We assume that the contact angle $\theta = \pi/2$.

The gradient of soil water pressure ∇p_w is assumed to be constant, as in [22]. Such gradients emerge due to, for example, an increase in the disjoining and capillary pressure caused by the above-mentioned gradual "evaporative thinning" (that is, the decrease of r_2 and increase of r_1 in the Of direction) of the water bridges. A higher evaporation rate from menisci of larger diameters (just above the capillary fringe in desert solonchaks), as compared with the vicinity of the super hot desert surface, is well documented.

We introduce a complex physical coordinate $z = x + iy = re^{i\varphi}$. The water microfluidic velocity obeys the Poisson equation [6]: that is

$$\Delta u(r, \varphi) = \frac{\partial^2 u}{\partial r^2} + \frac{1}{r}\frac{\partial u}{\partial r} + \frac{1}{r^2}\frac{\partial^2 u}{\partial \varphi^2} = -e, \quad e = \nabla p_w / \mu_w, \qquad (2.1)$$

where μ_w is the viscosity of the pore water. The right-hand side, e, in equation (2.1) is a given constant as a model hydrodynamic input (see [22, 25] for more details of similar flows in a circular digon and triangle).

The domain G_z in Figure 1(c) is a curvilinear tetragon made of two straight segments DC and BA and two arcs AMD and CND. At the boundary of G_z, the following conditions hold:

$$\begin{aligned} u(re^{\pm i\alpha/2}) &= 0 \quad r_1 < r < r_2, \\ \frac{\partial u(r_k e^{i\varphi})}{\partial r} &= 0 \quad k = 1, 2, \quad -\alpha/2 < \varphi < \alpha/2, \end{aligned} \qquad (2.2)$$

where r is a radial coordinate from the corner O and φ is an angular coordinate counted from the axis of symmetry of the bridge, that is, OMN. The pair r_1 and r_2 provide another geometrical input of our model. The no-slip (the first line in equation (2.1))
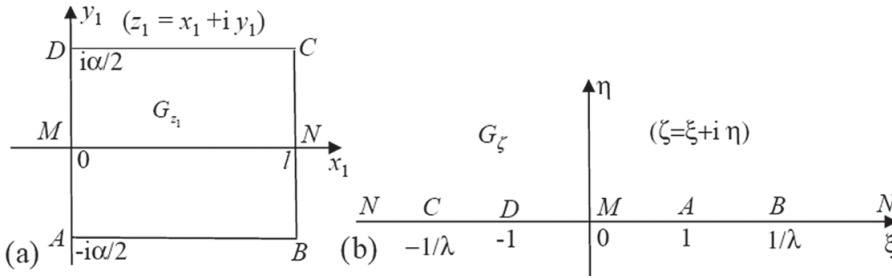
FIGURE 2. (a) Rectangle G_{z_1}. (b) Reference half-plane G_ζ.

and no-shear-stress (second line) conditions physically mean that the rigid skeleton of our porous medium is static (always true) and μ_a is almost zero, as was assumed in [22]. The latter assumption is justified by the two-order difference in viscosities of air and pore water. The main output of the model given by (2.1)–(2.2) is the velocity distribution $u(r, \varphi)$ and ensuing areal integral of this quantity over G_z, which gives the volumetric flow rate, and hence the water phase permeability. Extension of the model given by (2.1)–(2.2) to more complex menisci can be found in [15] among other applications to microgravity and soil physics.

The solution of a BVP with the $u = 0$ condition along the whole wall of our G_z was obtained by Sparrow et al. [32], and it was reported by Shah and London [31]. Unfortunately, no details of the solution are presented in [31, 32]. Moreover, equation (394) in [31] does not match equation (7) in [32]. Sparrow et al. used the method of separation of variables for solving their BVP for a harmonic function obeying Dirichlet''s boundary conditions, that is, they did not use the theory of holomorphic functions.

Aver'yanov''s [4] solution to PDE (2.1) can be readily reformulated for G_z in the following manner: the boundary conditions are no slip along DA in Figure 1(c) and no shear along DC, CB and CA.

Similar to the work in the papers [21, 22, 32], we reduce the BVP (2.1)–(2.2) for the Poisson equation to a BVP for the Laplace equation. For this purpose, we use the transformation

$$z_1 = \log(z/r_1) = x_1 + iy_1 = \log(r/r_1) + i\varphi, \quad x_1 = \log(r/r_1), \quad y_1 = \varphi,$$

$$\Phi(z) = u(r, \varphi) + er^2/4, \quad \Phi_1(z_1) = \Phi(r_1 \exp z_1), \tag{2.3}$$

which makes the function u in equation (2.1) harmonic in a rectangle G_{z_1} (Figure 2(a)): that is,

$$\Delta\Phi_1(x_1, y_1) = 0 \quad \text{for} \quad z_1 = x_1 + iy_1 \in G_{z_1}. \tag{2.4}$$

The boundary conditions (2.2), (2.3) in G_{z_1} become

$$AB, DC : \Phi_1(x_1, \pm\alpha) = 0.25 \, e \, r_1^2 e^{2x_1} \quad 0 < x_1 < l = \log(r_2/r_1),$$

$$AD : \frac{\partial \Phi_1(0, y_1)}{\partial x_1} = \frac{e \, r_1^2}{2} \quad -\alpha/2 < y_1 < \alpha/2,$$ (2.5)

$$BC : \frac{\partial \Phi_1(l, y_1)}{\partial x_1} = \frac{e \, r_2^2}{2} \quad -\alpha/2 < y_1 < \alpha/2.$$

Clearly, the function $\Phi_1(x_1, -y_1)$ is a solution of the mixed BVP (2.4) and (2.5) together with $\Phi_1(x_1, y_1)$. Hence,

$$\Phi_1(x_1, -y_1) = \Phi_1(x_1, y_1),$$

due to the uniqueness theorem [18].

Next, we introduce the complex potential function

$$\Omega_1(z_1) = \Phi_1(x_1, y_1) + i\Psi_1(x_1, y_1),$$ (2.6)

which is holomorphic in G_{z_1}. Here the function $\Psi_1(x_1, y_1)$, being complex conjugate to $\Phi_1(x_1, y_1)$, satisfies the symmetry condition

$$\Psi_1(x_1, -y_1) = -\Psi_1(x_1, y_1).$$

Due to equations (2.5) and the Riemann–Schwartz symmetry principle [17], the function (2.6) admits analytic continuations through the vertical sides of the boundary of the rectangle G_{z_1}. Hence, the Cauchy–Riemann conditions (CRC) hold up to these sides. Using the CRC $\partial \Phi_1/\partial x_1 = \partial \Psi_1/\partial y_1$ and the last two conditions of (2.5) and integrating, we get

$$\Psi_1(0, y_1) = 0.5er_1^2 y_1, \quad \Psi_1(l, y_1) = 0.5er_2^2 y_1 \quad -\alpha < y_1 < \alpha.$$ (2.7)

It is noteworthy that an arbitrary constant arising after integrating the CRC condition is equal to zero due to the above-mentioned symmetry property of the function $\Psi_1(x_1, y_1)$.

We map conformally G_{z_1} onto the upper half-plane $\text{Im}\zeta > 0$, $G_\zeta = \mathbb{C}^+$ (Figure 2(b)), with the correspondence of the points

$$C \to -1/\lambda, \quad D \to -1, \quad A \to 1, \quad B \to 1/\lambda,$$

where $0 < \lambda < 1$. The Schwarz–Christoffel formula [26] gives

$$z_1(\zeta) = -\frac{i\alpha}{2K(\lambda)} \int_0^\zeta \frac{dt}{\sqrt{(1 - t^2)(1 - \lambda^2 t^2)}} = -\frac{i\alpha}{2K(\lambda)} \text{F}(\arcsin \zeta, \lambda),$$ (2.8)

where $\text{F}(\arcsin \zeta, \lambda)$ and $K(\lambda)$ are, respectively, incomplete and complete elliptic integrals of the first kind (see [1, formulae 17.2.7, 17.3.1]). The modulus λ is determined from the condition

$$K'(\lambda)/K(\lambda) = 2l/\alpha,$$ (2.9)

where $K'(\lambda) = K(\lambda')$, $\lambda' = \sqrt{1 - \lambda^2}$. We use the `FindRoot` routine of MATHEMATICA [36] and find λ from equation (2.9).

Combining conditions (2.5) and (2.7), we obtain the following mixed BVP for the function $\Omega(\zeta) = \Omega_1(z(\zeta))$ in G_ζ

$$
\begin{aligned}
\mathrm{Re}\,\Omega(\xi) &= 0.25 e r_1^2 e^{2x_1(\xi)} & 1 < |\xi| < 1/\lambda, \\
\mathrm{Im}\,\Omega(\xi) &= 0.5 e r_1^2 y_1(\xi) & -1 < \xi < 1, \\
\mathrm{Im}\,\Omega(\xi) &= 0.5 e r_2^2 y_1(\xi) & |\xi| > 1/\lambda.
\end{aligned}
\tag{2.10}
$$

Here $x_1(\xi)$ and $y_1(\xi)$ are real and imaginary parts of the function (2.8), respectively: that is,

$$
x_1(\xi) = \frac{\alpha}{2K(\lambda)} \int_1^\xi \frac{dt}{\sqrt{(t^2 - 1)(1 - \lambda^2 t^2)}} = \frac{\alpha}{2K(\lambda)} F\!\left(\arcsin \frac{\sqrt{1 - \xi^{-2}}}{\lambda'}, \lambda'\right) \quad 1 < \xi < 1/\lambda,
$$

$$
y_1(\xi) = -\frac{\alpha}{2K(\lambda)} \int_0^\xi \frac{dt}{\sqrt{(1 - t^2)(1 - \lambda^2 t^2)}} = \frac{\alpha}{2K(\lambda)} F(\arcsin \xi, \lambda) \quad -1 < \xi < 1,
$$

$$
y_1(\xi) = \frac{\alpha}{2K(\lambda)} \int_{1/(\lambda\xi)}^1 \frac{dt}{\sqrt{(1 - t^2)(1 - \lambda^2 t^2)}} - \frac{\alpha}{2}
$$

$$
= \frac{\alpha}{2K(\lambda)} F\!\left(\arcsin \sqrt{\frac{\xi^2 - 1/\lambda^2}{\xi^2 - 1}}, \lambda\right) - \frac{\alpha}{2} \quad \xi > 1/\lambda.
$$

$$\tag{2.11}$$

It is clear that $x_1(\xi) = x_1(-\xi)$ for $-1/\lambda < \xi < -1$ and $y_1(\xi) = -y_1(-\xi)$ for $\xi < -1/\lambda$.

Thus, we have to find $\Omega(\zeta)$, which is holomorphic in G_ζ. This function must satisfy boundary conditions (2.10). It must be bounded at all transition points ± 1, $\pm 1/\lambda$ and at infinity in Figure 2(b). The index of the BVP (2.10) in the indicated class of functions is -2, and, generally speaking, one solvability condition must be satisfied [17]. As will be shown below, this solvability condition takes place automatically due to the properties of functions (2.11).

Solution of problem (2.10) bounded at transition points, but generally, not at infinity, [18] is

$$
\Omega(\zeta) = \frac{e r_1^2 \omega(\zeta)}{2\pi} \left(\int_{-1}^1 \frac{y_1(\xi)}{\omega(\xi)} \frac{d\xi}{\xi - \zeta} + \int_{L_\lambda} \frac{e^{2x_1(\xi)}}{2|\omega(\xi)|} \frac{d\xi}{\xi - \zeta} + e^{2l} \int_{1/\lambda}^{-1/\lambda} \frac{y_1(\xi)}{\omega(\xi)} \frac{d\xi}{\xi - \zeta} \right),
$$

where $L_\lambda = (-1, -1/\lambda) \cup (1, 1/\lambda)$, and the last integral is taken from $1/\lambda$ to $-1/\lambda$ through infinity. The branch of the function

$$
\omega(\zeta) = \sqrt{(1 - \zeta^2)(1 - \lambda^2 \zeta^2)},
\tag{2.12}
$$

is fixed in the upper half-plane by the condition of its positivity in the interval (-1,1). This branch is real and negative at $\zeta = \xi \in (-\infty, -1/\lambda) \cup (1/\lambda, \infty)$. The branch is pure

imaginary with negative and positive imaginary parts at the intervals $(1, 1/\lambda)$ and $(-1/\lambda, -1)$, respectively. It may seem that the $\Omega(\zeta)$ obtained in equation (2.12) is unbounded at infinity. If, however, we take into account the properties of functions (2.11) and (2.12), this solution can be rewritten as

$$\Omega(\zeta) = \frac{er_1^2\omega(\zeta)}{\pi}\left(\int_0^1 \frac{\xi y_1(\xi)}{\omega(\xi)}\frac{d\xi}{\xi^2 - \zeta^2} + \frac{1}{2}\int_1^{1/\lambda}\frac{\xi e^{2x_1(\xi)}}{|\omega(\xi)|}\frac{d\xi}{\xi^2 - \zeta^2} + e^{2l}\int_{1/\lambda}^\infty \frac{\xi y_1(\xi)}{\omega(\xi)}\frac{d\xi}{\xi^2 - \zeta^2}\right).$$
(2.13)

From equation (2.13), it is clear that our solution is bounded at $\zeta \to \infty$, as it should be. Note that the functions (2.8), (2.12) and (2.13) satisfy the same symmetry condition

$$z_1(\zeta) \equiv \overline{z_1(-\bar\zeta)}, \quad \omega(\zeta) \equiv \overline{\omega(-\bar\zeta)}, \quad \Omega(\zeta) \equiv \overline{\Omega(-\bar\zeta)}.$$
(2.14)

The total flow rate through G_z, due to equation (2.3), is

$$Q = \int_{G_z} u(x, y)\, ds = \int_{G_z} \Phi(x, y)\, ds - \frac{e\alpha}{16}(r_2^4 - r_1^4).$$

The last integral can be transformed as

$$Q_0 = \int_{G_z} \Phi(x, y)\, ds = \frac{i}{2}\int_{G_z} \Phi(x, y)\, dz \wedge d\bar z = \frac{ir_1^2}{2}\int_{G_{z_1}} \Phi_1(x_1, y_1)e^{2x_1}\, dz_1 \wedge d\bar z_1,$$

where $\wedge$ is the symbol for the exterior or wedge product. Using the transformation (2.8), we obtain

$$Q_0 = \frac{ir_1^2\alpha^2}{16K^2}\int_{\mathbb{C}^+}\frac{\Omega(\zeta) + \overline{\Omega(\zeta)}}{\omega(\zeta)\overline{\omega(\zeta)}}e^{2\mathrm{Re}z_1(\zeta)}\, d\zeta \wedge d\bar\zeta = \frac{r_1^2\alpha^2}{4K^2}\int_{-\infty}^\infty\int_0^\infty\frac{\mathrm{Re}\,\Omega(\xi + i\eta)}{|\omega(\xi + i\eta)|^2}e^{2x_1(\xi+i\eta)}\, d\eta\, d\xi.$$
(2.15)

Using the Stokes formula, Q_0 is transformed into a contour integral along the real axis

$$Q_0 = \frac{ir_1^2\alpha^2}{16K^2}\left(\int_{-\infty}^\infty\frac{\overline{e^{z_1(\xi)}}}{\omega(\xi)}\int_0^\xi\frac{\Omega(t)e^{z_1(t)}}{\omega(t)}dt\, d\xi - \int_{-\infty}^\infty\frac{e^{z_1(\xi)}}{\omega(\xi)}\int_0^\xi\frac{\overline{\Omega(t)e^{z_1(t)}}}{\overline{\omega(t)}}dt\, d\xi\right).$$

Finally, using the symmetry properties (2.14), we obtain

$$Q = -\frac{r_1^2\alpha^2}{4K^2}\mathrm{Im}\int_0^\infty\frac{\overline{e^{z_1(\xi)}}}{\overline{\omega(\xi)}}\int_0^\xi\frac{\Omega(t)e^{z_1(t)}}{\omega(t)}dt\, d\xi - \frac{e\alpha}{16}(r_2^4 - r_1^4).$$
(2.16)

We used the `NIntegrate` routine of Wolfram''s MATHEMATICA [36] to compute the integrals in equations (2.15) and (2.16). It turned out that computation Q using equation (2.16) required up to three days (for example, on a PC `Intel(R) Core(TM) i7-4770 CPU 3.40GHz, 3401 IHz, cores: 4, logical processors: 8`, which we used) for each value of r_1. If one uses equation (2.15) (as we did) the computations take up to an hour.

We introduce the dimensional quantities $Q^* = Q/(er_2^4)$ and $r^* = r_1/r_2$. Table 1 presents the values of Q^* for $\alpha = \pi/3$ and five values of r^*.

TABLE 1. Dimensionless flow rate Q^* computed using equations (2.15) and (2.16) for tetragons G_z having $\alpha = \pi/3$ and five values of r^*.

r^*	0.5	0.6	0.7	0.8	0.9
Q^*	0.02032	0.01952	0.01756	0.01389	0.00445

REMARK 1. In addition, for simplification of the expression $\Omega(\zeta)$ in equation (2.15), we used the substitution $\xi \rightarrow -1/(\lambda\xi)$ and transformed the last term in equation (2.13) to give

$$e^{2l} \int_{1/\lambda}^{\infty} \frac{\xi y_1(\xi)}{\omega(\xi)} \frac{d\xi}{\xi^2 - \zeta^2} = e^{2l} \int_{-\infty}^{-1/\lambda} \frac{\xi y_1(\xi)}{\omega(\xi)} \frac{d\xi}{\xi^2 - \zeta^2} = -\lambda e^{2l} \int_0^1 \frac{\xi y_1(\xi)}{\omega(\xi)} \frac{d\xi}{1 - \lambda^2 \xi^2 \zeta^2}.$$

To obtain this result, we used the identities

$$\omega(-1/(\lambda\zeta)) \equiv -\omega(\zeta)/(\lambda\zeta^2), \quad z_1(-1/(\lambda\zeta)) \equiv l - z_1(\zeta).$$

3. Other applications of water flow at high S_w in the pore core with static air in the corners

A curvilinear tetragon, as considered in Section 2 for the case of "thin bridges" and small S_w, can be used as a generic mobile phase conduit in the opposite limit of large S_w (close to 1). Indeed, let viscous water occupy almost the whole pore (see an equilateral triangle in Figure 3(a)) and move in the Of direction (not shown in Figure 3). Tiny pockets of immobile air are "entrapped" near the three corners in Figure 3(a) (see [9]) which, in applications to reservoir engineering, can be considered (at the REV-scale) as an early (primary) stage of crude oil recovery with a minor proportion of gas formation in the rock. The water flow domain in Figure 3(a) is a circular sextagon, with point E being its centre. Owing to symmetry, we can consider the curvilinear pentagon ADE_CEE_BA, that is, the third part of G_z in Figure 3(a). Along the broken line E_CEE_B the shear stress is zero (owing to symmetry). We can approximate this curvilinear pentagon DE_CEE_BA by a curvilinear tetragon DE_CNE_BA, in which the wedge E_CEE_B is replaced by a circular arc E_CNE_B, that is, we arrive at G_z in our Figure 1. Consequently, in ADE_CNE_BA of Figure 3, all analysis in Section 2 is valid.

In Figure 3(b), another limiting case of very low S_w is depicted. Now the pore gas is moving in the Of direction. The right-hand side in equation (2.1) becomes $e = \nabla p_a/\mu_a$, where μ_a is the viscosity of the air and ∇p_a is the gradient of the gas pressure along the pore. Water in Figure 3(b) is entrapped near the triangle corners, that is, it is immobile. Similarly to the case in Figure 3(a), we make a circular tetragon with mixed boundary conditions on its sides such that the analysis in Section 2 is valid. Applications of this pore-scale model are to the emission of in-pore CO_2 from the root zone, which has much higher concentrations of CO_2 than the superjacent atmospheric air. Evaluation of the fluxes of gases through the vadose zone are of utmost importance
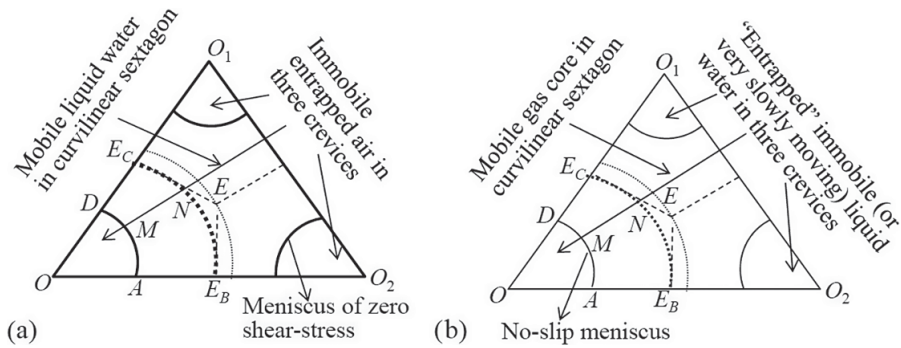
FIGURE 3. (a) Flow of water at high S_w in a cylindrical pore channel, the cross-section of which is an equilateral triangle with immobile air pockets entrapped near the corners. (b) Flow of air at low S_w in a cylindrical pore channel, the cross-section of which is an equilateral triangle with immobile water pockets entrapped near the corners.

(see [8, 30]), especially in the context of the impact of allegedly deleterious greenhouse gases (generated by rhizomes in the soil) on the human race and terrestrial ecosystems.

4. Concluding remarks on limitations and perspectives of our model

Our model and machinery of solving mixed BVPs for holomorphic functions allows us to use a combination of slip and no-slip boundary conditions, which is applicable when one phase is an immobile gas while the pore is polygonal rather than the Aver"yanov variably wet circle. In other words, we extend the cases of digon and trigon with mixed boundary conditions, considered in [22, 25], to the case of a circular tetragon, on the opposite sides of which these conditions are imposed. The motion of moisture in a "bridge", which is modelled by such a tetragon, is described by Poisson's equation. With the help of the Keldysh–Sedov-type formula [18], we obtained an integral representation for the in-pore velocity.

We have doubts about the solution obtained by Sparrow et al. [32] to the BVP with $u = 0$ on the whole boundary of the tetragon in Figure 1(c). The lack of comparisons in [32] (as well as in [31]) with the earlier explicit solution to the Poisson equation in a circular triangle, obtained by Saint–Venant [34] is confusing. Indeed, the solution obtained in [32] should degenerate into Saint–Venant's solution when the small-radius meniscus in Figure 1 vanishes, which was not demonstrated by Sparrow et al. [32].

The estimates of the flow rate Q through polygonal cross-sections with no-shear menisci can be attempted with the help of isoperimetric inequalities [27].

Recent video recording techniques of microfluidics processes can be used as experimental tools for measuring the in-pore parameters α, r_1, r_2 in Figure 1.

Solute transport on the microscale was not studied in our paper. In future, the advective dispersion equation on the macroscale (see [5]) can be downscaled to the pore level. The root zone salinization, caused by evapotranspiration from shallow water

tables, is a daunting problem in Australia and other arid countries, where applied mathematicians may, like Aver′yanov, transcend from microfluidics to the scale of engineered drainage of large salinized crop fields.

The limitations of our flow model in Section 2 are as follows.

(1) Viscosity of water is constant (in reality, it varies along the Of-axis, because the soil temperature of deserts has a strong diurnal gradient in the vertical direction).

(2) The flow domain G_z does not vary in the Of direction (in reality, water evaporates into the pore air and G_z dwindles from the capillary fringe to the topsoil).

(3) The water pressure gradient is constant (in reality, it is not because the decrease of r_1 and r_2) in the Of direction causes variation of this gradient.

(4) The pores are cylindrical and flow is two-dimensional (in reality, the pores are not cylindrical and flow is microscopically three-dimensional).

(5) The contact angle is 90° (in reality, most soils are either hydrophilic or hydrophobic).

(6) In Section 2, air is immobile (in reality, both water and air move, and not always co-currently).

(7) Water "bridges" are assumed to be stable to potential perturbations (in reality, the menisci in Figure 1 may break into Avery′anov-type films that simply "coat" the wall of the polygonal pore, which gives the case of flow considered by Kacimov et al. [22]).

(8) Gravity is ignored, that is, capillarity dominates the fluid behaviour, along with the hydrodynamic pressure gradient along Of (in thick vadose zones, the gravity force is explicitly counted on the right-hand side of the Poisson equation).

(9) Menisci are circular arcs (in reality, they are not [15]).

Acknowledgements

References

[1]   M. Abramowitz and I. A. Stegun, *Handbook of mathematical functions with formulas, graphs, and mathematical tables* (National Bureau of Standards, Washington, DC, 1964).

[2]   M. Al-Battashi, A. Al-Maktoumi, A. Kacimov, A. Al-Mayahi, A. Al-Shukaili and S. Al-Ismaily, "Shallow water table in arid urban zone: preliminary study at Sultan Qaboos University campus, Oman", *J. Agric. Marine Sci.* **27**(1) (2022) 62–76; doi:10.53541/jams.vol27iss1pp62-76.

[3]   M. B. Allen, *The mathematics of fluid flow through porous media* (Wiley, Hoboken, NJ, 2021).

[4]   S. F. Aver'yanov, "Dependence of soil water permeability on air content", *Doklady AN SSSR* **69** (1949) 142–144 (in Russian).

[5]   S. F. Aver'yanov, *Combating salinization of irrigated lands* (Kolos, Moscow, 1978) (in Russian).

[6] F. G. Avkhadiev and A. R. Kacimov, "Analytical solutions and estimates for microlevel flows", *J. Porous Media* **8** (2005) 125–148; doi:10.1615/JPorMedia.v8.i2.30.

[7] F. G. Avkhadiev and A. R. Kacimov, "The Saint–Venant type isoperimetric inequalities for assessing saturated water storage in Lacunary shallow perched aquifers", *Z. Angew. Math. Mech. – J. Appl. Math. Mech.* **103** (2023) Article ID: e202100069; doi:10.1002/zamm.202100069.

[8] I. Ben-Noah and S. P. Friedman, "Review and evaluation of root respiration and of natural and agricultural processes of soil aeration", *Vadose Zone J.* **17** (2018) 1–47; doi:10.2136/vzj2017.06.0119.

[9] M. J. Blunt, *Multiphase flow in permeable media: a pore-scale perspective* (Cambridge University Press, Cambridge, 2017); doi:10.1017/9781316145098.

[10] V. T. Buchwald and F. Viera, "Linearised evaporation from a soil of finite depth above a water table", *ANZIAM J.* **39** (1998) 557–576; doi:10.1017/S0334270000007803.

[11] R. Chhabra, *Salt-affected soils and marginal waters: global perspectives and sustainable management* (Springer, Cham, 2022).

[12] B. Daneshian, G. Habibagahi and E. Nikooee, "Determination of unsaturated hydraulic conductivity of sandy soils: a new pore network approach", *Acta Geotechnica* **16** (2021) 449–466; doi:10.1007/s11440-020-01088-3.

[13] F. A. L. Dullien, *Porous media: fluid transport and pore structure*, 2nd edn (Academic Press, New York, 1992).

[14] N. A. El-Khatib, "The relative permeabilities of an idealized model of two-phase flow in porous media", *Appl. Math. Model.* **4** (1980) 463–466; doi:10.1016/0307-904X(80)90179-1.

[15] R. Finn, *Equilibrium capillary surfaces* (Springer, New York, 1986); doi:10.1007/978-1-4613-8584-4.

[16] D. G. Fredlund and H. Rahardjo, *Soil mechanics for unsaturated soils* (Wiley, New York, 1993); doi:10.1002/9780470172759.

[17] F. D. Gakhov, *Boundary value problems* (Addison Wesley, New York, 1966).

[18] P. Henrici, *Applied and computational complex analysis, volume 3. Discrete Fourier analysis, Cauchy integrals, construction of conformal maps, univalent functions* (Wiley, New York, 1993).

[19] A. Kacimov, "Analytic solutions for quasi-3D seepage in a shallow unconfined aquifer as a plane composed of a transpiration-inducing park and its hydraulically commingled exterior", *J. Hydrology* **626** (2023) Article ID: 130302; doi:10.1016/j.jhydrol.2023.130302.

[20] A. Kacimov, A. Al-Maktoumi, S. Al-Ismaily, A. Al-Mayahi, A. Al-Shukaili, Yu. Obnosov and A. Osman, "Water table rise in arid urban area due to evaporation impedance and its mitigation by intelligently designed capillary chimney siphons", *Environ. Earth Sci.* **80** (2021) 1–17; doi:10.1007/s12665-021-09857-3.

[21] A. Kacimov, N. D. Yakimov and J. Šimůnek, "Phreatic seepage flow through an earth dam with an impeding strip", *Comput. Geosci.* **24** (2020) 17–35; doi:10.1007/s10596-019-09879-8.

[22] A. R. Kacimov, D. V. Maklakov, I. R. Kayumov and A. Al-Futaisi, "Free surface flow in a microfluidic corner and in an unconfined aquifer with accretion: the Signorini and Saint–Venant analytical techniques revisited", *Transp. Porous Media* **116** (2017) 115–142; doi:10.1007/s11242-016-0767-y.

[23] V. A. Kovda, *Fundamental theory on soils. General theory of Pedogenic process* (Nauka, Moscow, 1973) (in Russian).

[24] J. R. Philip, "Flow in porous media", *Annu. Rev. Fluid Mech.* **2** (1970) 177–204; doi:10.1146/annurev.fl.02.010170.001141.

[25] J. R. Philip, "Flows satisfying mixed no-slip and no-shear conditions", *J. Appl. Math. Phys. (ZAMP)* **23** (1972) 353–372; doi:10.1007/BF01595477.

[26] P. Y. Polubarinova-Kochina, *Theory of ground water movement* (Princeton University Press, Princeton, NJ, 1962), (Second edition of the book (in Russian) published in 1977, Nauka, Moscow).

[27] G. Pólya and G. Szegö, *Isoperimetric inequalities in mathematical physics* (Princeton University Press, Princeton, NJ, 1951).

[28] D. E. Radcliffe and J. Šimůnek, *Soil physics with HYDRUS: modeling and applications* (CRC Press, Boca Raton, FL, 2018); doi:10.1201/9781315275666.

[29] A. N. Salugin, "Modeling the evaporation process", *Arid Ecosystems* **13** (2023) 133–139; doi:10.1134/S2079096123020129.

[30] B. R. Scanlon, J. P. Nicot and J. W. Massmann, "Soil gas movement in unsaturated systems", in: *Soil physics companion* (ed. A. W. Warrick) (CRC Press, Boca Raton, FL, 2022) 297–341.

[31] R. K. Shah and A. L. London, *Laminar flow forced convection in Ducts: a source book for compact heat exchanger analytical data* (Academic Press, New York, 1978).

[32] E. M. Sparrow, T. S. Chen and V. K. Jonsson, "Laminar flow and pressure drop in internally finned annular ducts", *Inter. J. Heat Mass Transfer* **7** (1964) 583–585; doi:10.1016/0017-9310(64)90056-0.

[33] P. J. Thorburn, "Land management impacts on evaporation from shallow, saline water tables", in: *Subsurface hydrological responses to land cover and land use changes* (ed. M. Taniguchi) (Springer, New York, 1997) 21–34; doi:10.1007/978-1-4615-6141-5.

[34] S. P. Timoshenko and J. C. Goodier, *Theory of elasticity* (McGraw-Hill, New York, 1970).

[35] G. J. Weir, "Linearised evaporation about a shallow half-plane pond", *ANZIAM J.* **34** (1993) 355–367; doi:10.1017/S0334270000008948.

[36] S. Wolfram, *Mathematica. A system for doing mathematics by computer* (Addison-Wesley, Redwood City, CA, 1991).